



Article

Improving Breakdown Voltage and Threshold Voltage Stability by Clamping Channel Potential for Short-Channel Power p-GaN HEMTs

Hongyue Wang ^{1,*}, Yijun Shi ¹, Yajie Xin ^{2,*}, Chang Liu ¹ , Guoguang Lu ¹ and Yun Huang ¹

¹ Science and Technology on Reliability Physics and Application of Electronic Component Laboratory, China Electronic Product Reliability and Environmental Testing Research Institute, Guangzhou 510610, China; syijun0119@163.com (Y.S.); xd_liuchang@163.com (C.L.); luguoguang@ceprei.com (G.L.); hyun@ceprei.com (Y.H.)

² State Key Laboratory of Electronic Thin Films and Integrated Devices, University of Electronic Science and Technology of China (UESTC), Chengdu 610054, China

* Correspondence: wanghongyue@pku.edu.cn (H.W.); 201811022423@std.uestc.edu.cn (Y.X.)

Abstract: This paper proposes a novel p-GaN HEMT (P-HEMT) by clamping channel potential to improve breakdown voltage (BV) and threshold voltage (V_{TH}) stability. The clamping channel potential for P-HEMT is achieved by a partially-recessed p-GaN layer (PR p-GaN layer). At high drain bias, the two-dimensional electron gas (2DEG) channel under the PR p-GaN layer is depleted to withstand the drain bias. Therefore, the channel potential at the drain-side of the p-GaN layer is clamped to improve BV and V_{TH} stability. Compared with the conventional p-GaN HEMT (C-HEMT), simulation results show that the BV is improved by 120%, and the V_{TH} stability induced by high drain bias is increased by 490% for the same on-resistance. In addition, the influence of the PR p-GaN layers' length, thickness, doping density on BV and V_{TH} stability is analyzed. The proposed device can be a good reference to improve breakdown voltage and threshold voltage stability for short-channel power p-GaN HEMTs.

Keywords: breakdown voltage; partially recessed; p-GaN HEMT; short-channel



Citation: Wang, H.; Shi, Y.; Xin, Y.; Liu, C.; Lu, G.; Huang, Y. Improving Breakdown Voltage and Threshold Voltage Stability by Clamping Channel Potential for Short-Channel Power p-GaN HEMTs. *Micromachines* **2022**, *13*, 176. <https://doi.org/10.3390/mi13020176>

Academic Editors: Benoit Bakeroot and Matteo Meneghini

Received: 26 December 2021

Accepted: 14 January 2022

Published: 25 January 2022

Publisher's Note: MDPI stays neutral with regard to jurisdictional claims in published maps and institutional affiliations.



Copyright: © 2022 by the authors. Licensee MDPI, Basel, Switzerland. This article is an open access article distributed under the terms and conditions of the Creative Commons Attribution (CC BY) license (<https://creativecommons.org/licenses/by/4.0/>).

1. Introduction

GaN-based devices are promising for next-generation high-efficiency, high-frequency, high-temperature, and high-power applications due to their superior material properties [1–8]. According to the application requirements, it is necessary to improve the electric performance of GaN devices [9].

For power applications, low on-resistance R_{on} and high breakdown voltage (BV) for GaN HEMTs are very desirable [7]. In order to realize low on-resistance, a short length scheme is always chosen as channel resistance under the gate is the main part of the total resistance for AlGaIn/GaN HEMTs [10]. However, the short channel GaN HEMTs often suffer from the adverse drain-induced barrier lowering (DIBL) effect [11], namely, degradation of forward-blocking characteristics and negative threshold voltage (V_{TH}) shift at high drain bias [12,13]. In order to suppress the DIBL effect-induced BV degradation, Pinchbeck et al. proposed a GaN HEMT with extended gate length to achieve reduced short channel effect and improved BV [14]. In addition, Lu et al. proposed a dual gate AlGaIn HEMT to achieve high BV, low on-resistance, and high threshold voltage characteristics [15]. However, those methods are not suitable for short-channel p-GaN HEMTs to suppress the BV degradation and V_{TH} instability, which owns a p-GaN layer to achieve enhancement-mode function.

In this work, we proposed a novel p-GaN HEMT to improve the BV and V_{TH} stability, which features a partially-recessed p-GaN layer. At high drain bias, the two-dimensional

electron gas (2DEG) channel under the partially-recessed p-GaN layer can withstand the high drain voltage to achieve higher BV and more stable V_{TH} for the short-channel p-GaN HEMTs. The paper is organized as follows: the device structure and operation mechanism of the proposed p-GaN HEMT are presented in Section 2; the simulation results and discussions are shown in Section 3; the conclusions are drawn in Section 4.

2. Device Structure and Mechanism

The schematic structure of the proposed p-GaN HEMT (P-HEMT) is shown in Figure 1b. Compared with conventional p-GaN HEMT (C-HEMT), the P-HEMT features a partially recessed layer (PR p-GaN layer). To illustrate the mechanism of improving BV and V_{TH} stability for the P-HEMT, we employ one equivalent model with two series HEMTs, which are defined as high threshold voltage HEMT1 and low threshold voltage HEMT2, as shown in Figure 2a. As the threshold voltage of HEMT1 (V_{TH1}) is larger than the threshold voltage of HEMT2 (V_{TH2}), HEMT2 has been turned on when the gate to source voltage (V_{GS}) is larger than V_{TH1} . Therefore, the threshold voltage V_{TH} of P-HEMT is mainly determined by V_{TH1} , namely, $V_{TH} \approx V_{TH1}$. The potential is defined as V_C at the connection node, which is also shown in Figure 1b. When $0 < V_C < V_{GS} - V_{TH2}$ (i.e., $V_{GS} - V_C > V_{TH2}$), HEMT2 is at on-state. Therefore, V_C increases with V_{DS} at low drain bias. When $V_C > V_{GS} - V_{TH2}$ (i.e., $V_{GS} - V_C < V_{TH2}$), HEMT2 is in an off-state and the 2DEG channel under the PR p-GaN layer is depleted to withstand V_{DS} voltage. Therefore, V_C is clamped and does not increase with V_{DS} at high drain bias, as the blue dash line shown in Figure 2b. As a result, the barrier height for electrons injecting from source to drain will be hardly influenced by high drain bias, which makes V_{TH} more stable. In addition, the stable barrier height leads to decreased electrons flowing from source to drain compared with C-HEMT at high drain bias, which induces delayed occurrence of avalanche breakdown, namely, improves breakdown voltage.

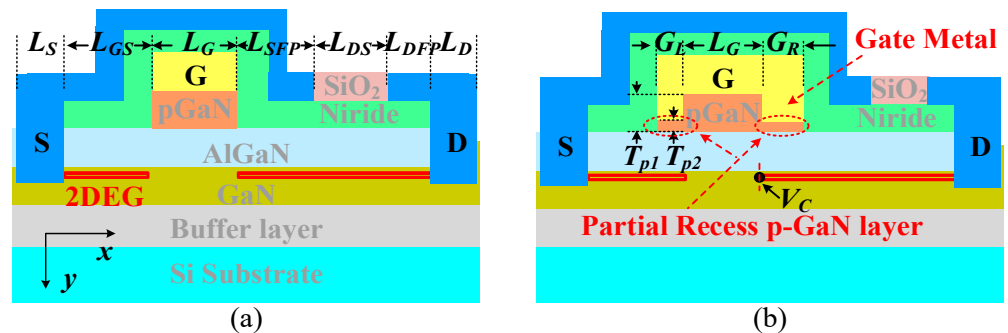


Figure 1. The schematic device structures of (a) conventional p-GaN HEMT (C-HEMT) and (b) proposed p-GaN HEMT (P-HEMT) with partially-recessed p-GaN layer (PR p-GaN layer).

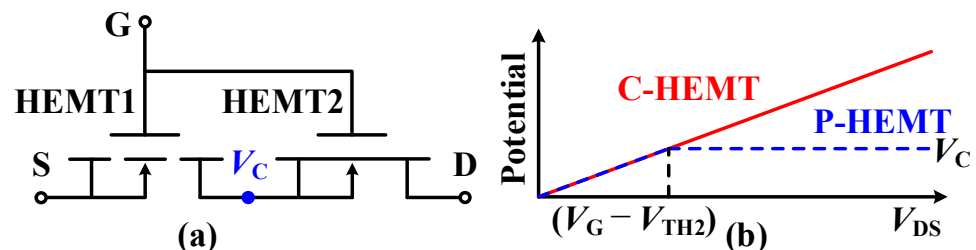


Figure 2. (a) The equivalent model of the P-HEMT with a high threshold voltage HEMT1 and a low threshold voltage HEMT2; (b) the potential V_C versus V_{DS} .

3. Results and Discussions

In this section, the current-voltage and capacitance-voltage characteristics of P-HEMT are investigated by Sentaurus TCAD simulation software [16], and the design considerations are also discussed. In the simulation, the optimized device parameters are as

listed in Table 1 unless otherwise specified, which is also based on our previous calibrated work [17]. In particular, the structure parameters of C-HEMT are designed according to the dissected cross-sectional scanning electron microscope (SEM) images. The x- and y-coordinates and the epitaxial structures of the two devices are illustrated in Figure 1 [18]. For C-HEMT, an ionized acceptor concentration $N_{\text{p-GaN}} = 3.5 \times 10^{17} \text{ cm}^{-3}$ is induced in the p-GaN layer with the $t_{\text{p-GaN}} = 50 \text{ nm}$, which contributes to V_{TH} and on-state current calibrations for the C-HEMT. In addition, the deep acceptor traps and self-compensating donor traps [19] are also considered in the AlGaIn buffer layer with an activation energy of $E_V + 0.9 \text{ eV}$ and $E_C - 0.11 \text{ eV}$ [20], and the trap density is $3 \times 10^{16} \text{ cm}^{-3}$ and $1.3 \times 10^{15} \text{ cm}^{-3}$ respectively [21]. Typically, the G_L of the PR layer on the source side is only set to $0.1 \mu\text{m}$ considering the deviation of the fabrication process, and it should be as small as possible to reduce the negative influence on input capacitance in practical application. The G_R of the PR layer on the drain side is an adjustable parameter as it makes obvious significance on the improvement of BV and V_{TH} stability. In this paper, the gate length L_G of C-HEMT is the same as the length of the thicker p-GaN layer of P-HEMT for achieving the same on-resistance, and the length of the partially-recessed p-GaN layer is not included in the nominal gate length L_G . Table 1 shows the calibrated results of the 100 V enhancement-mode p-GaN HEMT [22], and it can be seen that the results are in good agreement with the datasheet as shown in Figure 3. Typically, the BV characteristic considering the avalanche model [23] coincides well with the testing result.

Table 1. Device parameters specification.

Symbols	Definitions	Typical Value
L_S	Source length	$0.7 \mu\text{m}$
L_G	Gate length	$0.35 \mu\text{m}$
L_D	Source-to-gate length	$0.7 \mu\text{m}$
L_{GS}	Source-to-gate length	$0.4 \mu\text{m}$
L_{DS-C}	C-HEMT Gate-to-drain length	$1.95 \mu\text{m}$
L_{DS-PR}	P-HEMT Gate-to-drain length	$1.95 \mu\text{m}$
L_{SFP-C}	C-HEMT Source-field-plate length	$0.8 \mu\text{m}$
L_{SF-PR}	P-HEMT Source-field-plate length	$(0.8 - G_r) \mu\text{m}$
L_{DFP}	Drain-field-plate length	$0.25 \mu\text{m}$
t_{SiN}	Thickness of SiN	80 nm
t_{SiO_2}	Thickness of SiO ₂	270 nm
G_L	The left PR p-GaN length	$0.1 \mu\text{m}$
G_R	The right PR p-GaN length	$0.3 \mu\text{m}$
T_{p2}	Thickness of PR p-GaN	30 nm
T_{p1}	Thickness of p-GaN	50 nm
t_{ba}	Thickness of barrier	12.5 nm
t_{ch}	Thickness of channel	20 nm
t_{bu}	Thickness of buffer	$2 \mu\text{m}$
t_{nu}	Thickness of nucleation	10 nm
t_{sub}	Thickness of substrate	$550 \mu\text{m}$
t_{gate}	Thickness of Schottky gate	100 nm
χ_{ba}	Al composition of barrier	25%
χ_{bu}	Al composition of buffer	5%
W_G	Work-function of the gate	4.8 eV
N_{DT1}	Nitride/AlGaIn trap density	$3 \times 10^{13} \text{ cm}^{-2}$ ($E_C - 0.4 \text{ eV}$) [24]
N_{DTC}	Channel UID concentration	$1 \times 10^{15} \text{ cm}^{-3}$

Table 1. Cont.

Symbols	Definitions	Typical Value
N_{AT1}	Buffer acceptor trap density	$3 \times 10^{16} \text{ cm}^{-3}$ ($E_V + 0.9 \text{ eV}$) [17]
N_{DT2}	Buffer donor trap density	$1.3 \times 10^{15} \text{ cm}^{-3}$ ($E_C - 0.11 \text{ eV}$)
N_{AT2}	Silicon/AlN acceptor trap density	$3 \times 10^{13} \text{ cm}^{-2}$ ($E_C - 1.7 \text{ eV}$)
$N_{p\text{-GaN}}$	Activated Mg Doping	$3.5 \times 10^{17} \text{ cm}^{-3}$

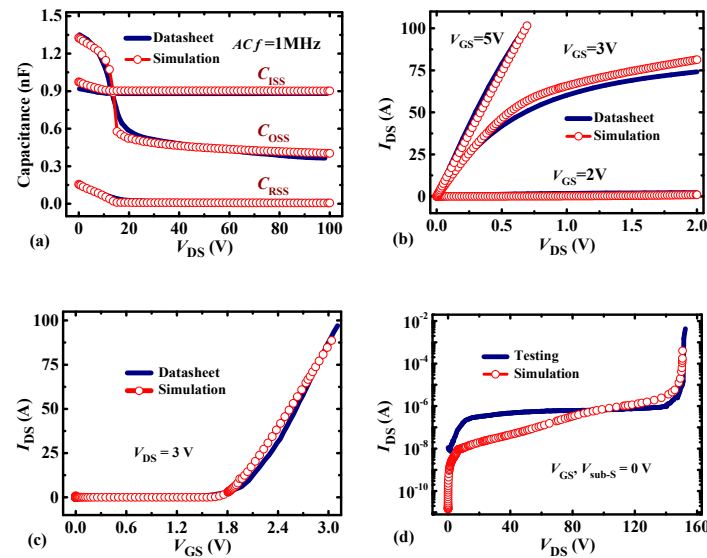


Figure 3. (a) Capacitance-Voltage characteristic; (b) output characteristic; (c) transfer characteristic; (d) forward-blocking characteristic. The forward-blocking characteristic is based on the testing data as there is no breakdown voltage result in the datasheet.

3.1. Static and Transient Characteristics

Figure 4 shows the forward-blocking and output characteristics of the P-HEMT. As shown in Figure 4a, it can be seen that the BV ($I_{DS_off} = 100 \mu\text{A}$) for the P-HEMT is increased by 120% compared with the 100 V C-HEMT, which mainly results from the delayed occurrence of avalanche breakdown. As shown in Figure 4b, it can be observed that impact ionization at the drain-side source field plate is decreased at the same 150 V drain bias, which results from the decreased electrons flowing from source to drain. In addition, as shown in Figure 4c, the conduction energy E_C level at the drain-side of the p-GaN layer for P-HEMT is clamped, which results from the clamped V_C as stated in section II. As shown in Figure 4d, for typical gate operation voltage $V_{GS} = 5 \text{ V}$, the output curves of C-HEMT and P-HEMT are coincident well, which indicates that the PR p-GaN layer makes a negligible impact on the on-state resistance. For $V_{GS} = 2 \text{ V}$, the I_{DS} for C-HEMT is slightly higher than P-HEMT, which results from the partial depletion of the 2DEG channel under the PR p-GaN layer.

Figure 5 shows the transfer characteristics of the P-HEMT. At low drain bias (such as $V_{DS} = 1 \text{ V}$), the transfer curves of C-HEMT and P-HEMT are coincident well and the threshold voltage difference is less than 0.05 V. However, with the increasing of V_{DS} , the V_{TH} of C-HEMT decreases obviously while V_{TH} of P-HEMT slightly reduced. Typically, the V_{TH} decrease from $V_{DS} = 1 \text{ V}$ to $V_{DS} = 50 \text{ V}$ is 0.59 V for C-HEMT and 0.1 V for P-HEMT, as shown in Figure 5b. The significantly decreased V_{TH} for C-HEMT will lead to false turn-on at high drain bias (typically, from off-state to on-state), which is not acceptable for practical application. However, from the results, it can be deduced that the P-HEMT with more stable V_{TH} can be contributed to alleviating this problem very well.

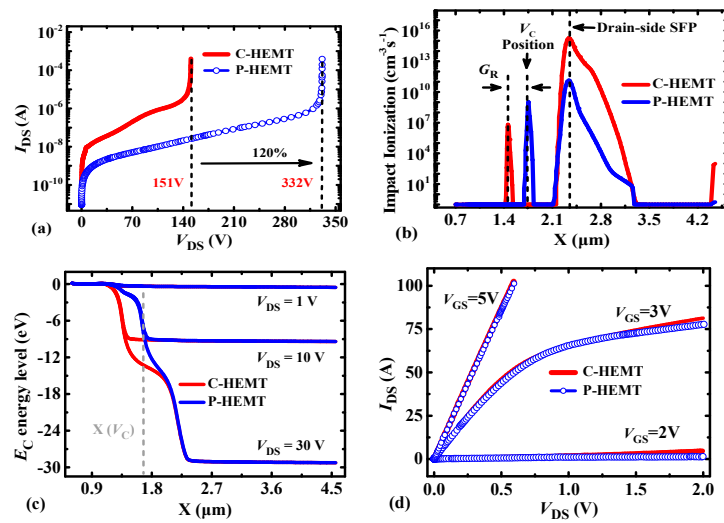


Figure 4. Comparison of the (a) forward-blocking characteristic, (b) impact ionization profile along the channel at $V_{DS} = 150$ V, (c) conduction energy level E_C profile along the channel, and (d) output characteristic between C-HEMT and P-HEMT.

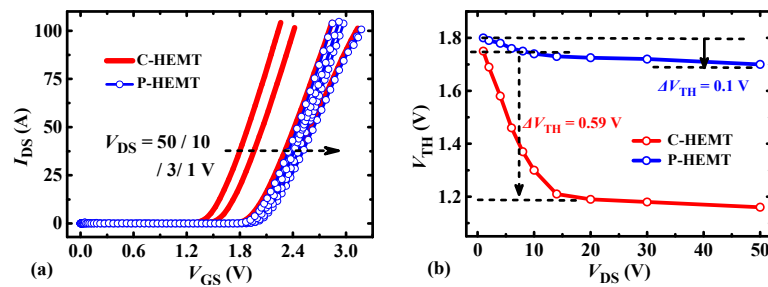


Figure 5. Comparison of (a) the transfer, (b) the threshold voltage V_{TH} (at $I_{DS} = 10$ mA) depending on V_{DS} between the C-HEMT and P-HEMT. For a fair comparison, the V_{TH} is defined when $I_{DS} = 10$ mA.

To illustrate the impact of the PR p-GaN layer on transient behavior, the simulation using a double pulse circuit is carried out, as shown in Figure 6. Compared with C-HEMT, the calculated turn-on loss and turn-off loss of P-HEMT are increased by $0.09 \mu\text{J}$ and $0.02 \mu\text{J}$ at 500 kHz respectively, and the total switching loss is increased by less than 7.8%. It can be inferred the increased switching loss mainly results from the increase of the input capacitance C_{ISS} . As shown in Figure 7, it can be seen that the off-state and on-state input capacitance C_{ISS} is increased by 18.9% and 47.2%, respectively. In addition, as shown in Figure 7a, the C_{OSS} at high-drain bias ($V_{DS} > 15$ V) is the same as C-HEMT, and the output capacitance C_{OSS} at a low-drain bias ($V_{DS} < 15$ V) is decreased by 16.7%, which mainly results from the depletion of 2DEG channel under the PR layer as stated in section II. The decrease of C_{OSS} at $V_{DS} < 15$ V is contributed to reducing the increment of switching loss.

3.2. Design Considerations of P-HEMT

This section mainly discusses the impact of PR p-GaN layers' thickness, length, and doping concentration on the BV and V_{TH} stability.

Figure 8 shows the V_{TH} and BV results for different thicknesses of the PR p-GaN layer. As shown in Figure 8a, it can be seen that the DIBL value is increased with PR p-GaN layer thickness. The DIBL parameter is defined as $(V_{TH}^{High} - V_{TH}^{Low}) / (V_{DS}^{High} - V_{DS}^{Low})$ to represent the V_{TH} stability, and the smaller value symbolizes the more stable V_{TH} . As shown in Figure 8b, it can be seen that the V_{TH} for different thickness PR layers from $V_{DS} = 1$ V to $V_{DS} = 50$ V decreases, but the difference is all less than 0.1 V, which indicates the high stable V_{TH} for P-HEMT. The log-scale transfer characteristics are as shown in Figure 8c–e. For the same drain bias, the V_{TH} slightly increases (≤ 0.05 V) with the thickness of the PR

p-GaN layer, which mainly results from the 2DEG depletion under the PR p-GaN layer. In addition, it can be observed that the BV is all larger than 320 V, which indicates the impact of the PR p-GaN layer’s thickness on BV is negligible. However, for a smaller thickness PR p-GaN layer, the gate-to-source breakdown voltage can be reduced. Figure 9a shows the I_{GS} — V_{GS} characteristics for 20/30/40 nm PR p-GaN layer, and it can be seen that the I_{GS} for $T_{p2} = 20$ nm abruptly increases when V_{GS} is larger than 5.1 V. To explore the origin of the abrupt I_{GS} , the current distribution of the three thickness PR p-GaN layer devices are plotted, as shown in Figure 9b–d. For the device with $T_{p2} = 20$ nm, the current density from the PR p-GaN layer to the 2DEG channel is larger than the normal thickness p-GaN layer. This indicates the high gate current mainly results from the breakdown of the PR p-GaN layer. As a comparison, the gate current density for $T_{p2} = 30/40$ nm is very small. Based on the above analysis, it can be deduced that the PR p-GaN layer thickness should be taken into careful consideration in the design to avoid gate breakdown.

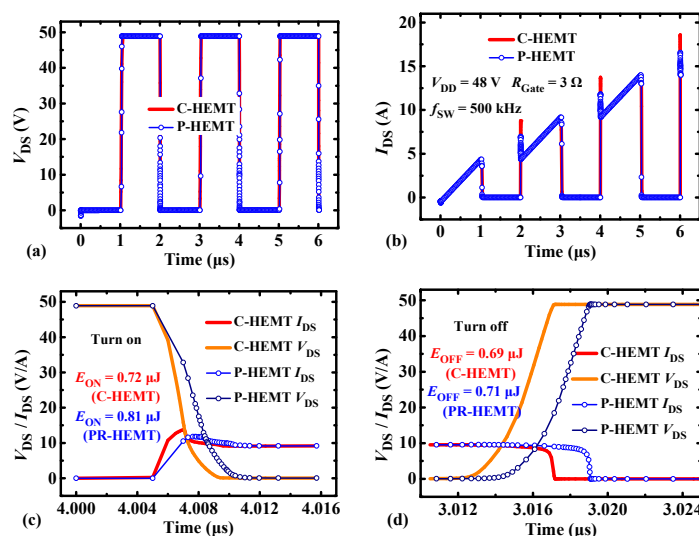


Figure 6. The switching transient comparison between C-HEMT and P-HEMT by double-pulse simulation. (a) V_{DS} voltage waveforms; (b) I_{DS} current waveforms; (c) turn on transient at ~ 10 A I_{DS} current; (d) turn off transient at ~ 10 A I_{DS} current.

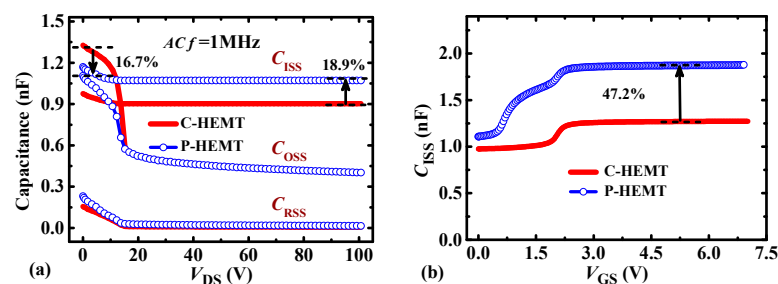


Figure 7. Comparison of (a) capacitance- V_{DS} , and (b) C_{ISS} - V_{GS} characteristics between C-HEMT and P-HEMT.

Figure 10 shows the impact of PR p-GaN layer length on the BV and V_{TH} characteristics. It can be seen that DIBL decreases with G_r , which indicates the V_{TH} stability is increased. However, the DIBL tends to be stable and the BV decreases when G_r is larger than $0.5 \mu\text{m}$. The decrease of the BV mainly results from the high electric field at the drain-side of the PR p-GaN layer, as shown in Figure 11. Therefore, it can be deduced that the PR p-GaN layer length should be in a reasonable range to get a good trade-off for V_{TH} stability and high BV. For the 100 V p-GaN HEMT discussed in this paper, the $0.3\text{--}0.5 \mu\text{m}$ PR p-GaN layer is recommended.

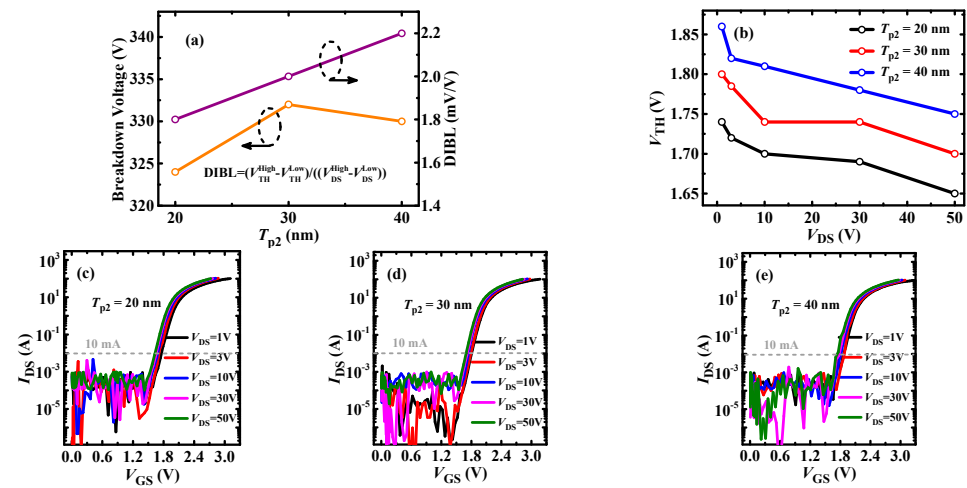


Figure 8. (a) Breakdown voltage (BV) and DIBL versus PR thickness; (b) the threshold voltage V_{TH} (at $I_{DS} = 10$ mA) depending on V_{DS} ; the transfer characteristics of P-HEMT with $T_{p2} =$ (c) 20 nm; (d) 30 nm; (e) 40 nm.

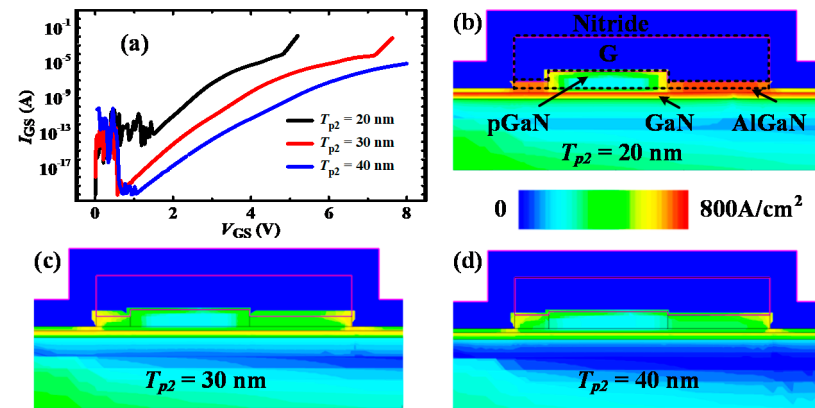


Figure 9. (a) The I_{GS} - V_{GS} characteristics of P-HEMT with different T_{p2} ; the current distribution at the gate part for $T_{p2} =$ (b) 20 nm, (c) 30 nm, (d) 40 nm.

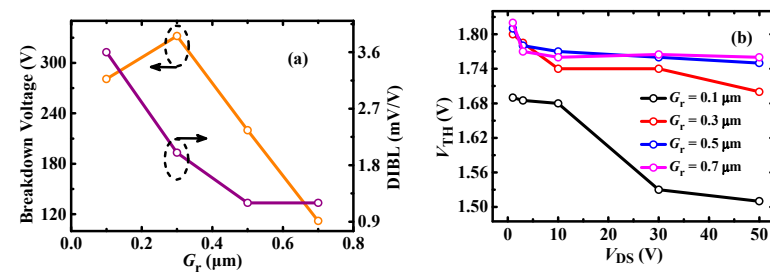


Figure 10. (a) BV and DIBL, (b) V_{TH} (at $I_{DS} = 10$ mA) depending on V_{DS} for different G_r length.

Figure 12 shows the impact of p-GaN doping density on the V_{TH} and BV. It can be observed that the p-GaN doping density mainly determines the magnitude of V_{TH} , and it makes a negligible effect on BV and DIBL. Figure 13 shows the V_{TH} and BV characteristics of P-HEMT with different gate lengths L_g . It can be seen that longer gate length induces higher V_{TH} , lower DIBL, which means longer gate length is contributed to making V_{TH} more stable. In addition, longer gate length induces higher BV, which mainly results from the electric field modulation. However, longer gate length will induce higher on-resistance. Therefore, the gate length should be taken into careful consideration to get a better trade-off for V_{TH} stability, BV, and R_{ON} .

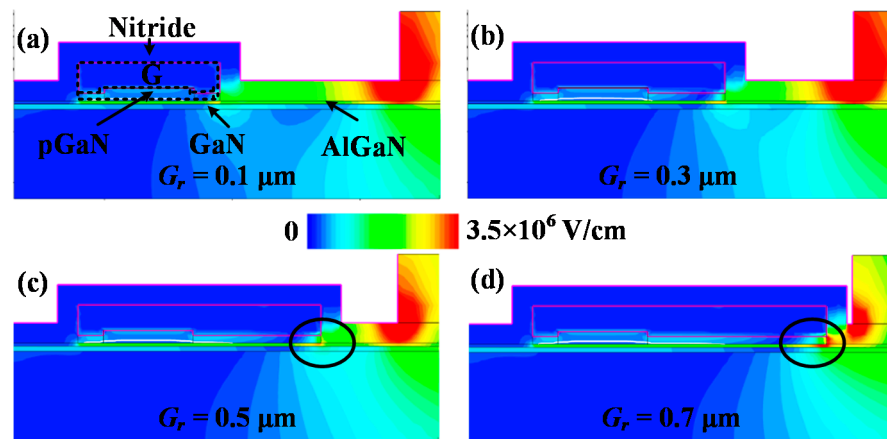


Figure 11. The electric field distribution of P-HEMT for $G_r =$ (a) $0.1 \mu\text{m}$; (b) $0.3 \mu\text{m}$; (c) $0.5 \mu\text{m}$; (d) $0.7 \mu\text{m}$ at breakdown voltage.

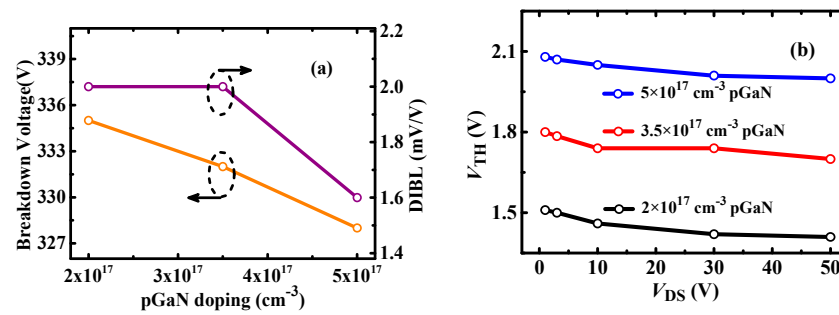


Figure 12. (a) BV and DIBL, (b) V_{TH} (at $I_{DS} = 10 \text{ mA}$) depending on V_{DS} for different p-GaN doping density.

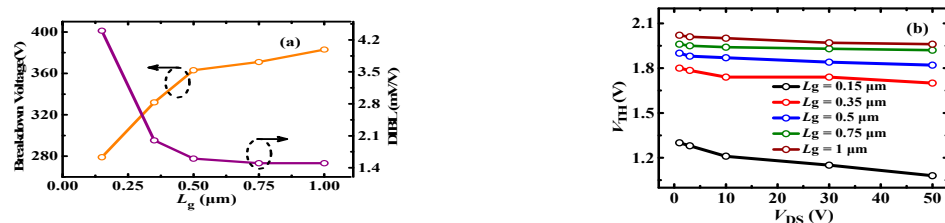


Figure 13. (a) BV and DIBL, (b) V_{TH} depending on V_{DS} for different gate lengths.

4. Conclusions

This paper proposes a novel p-GaN HEMT with a PR p-GaN layer to improve BV and V_{TH} stability. The device features a PR p-GaN layer compared with conventional p-GaN HEMT. At high drain bias, the two-dimensional electron gas channel under the PR p-GaN layer is depleted to withstand V_{DS} , thereby contributing to improving the BV and V_{TH} stability. Compared with the C-HEMT, simulation results show that the breakdown voltage is improved by 120%, and the V_{TH} stability changing with V_{DS} is increased by 490% (the decrease of V_{TH} at 50 V for P-HEMT and C-HEMT are 0.1 V and 0.59 V respectively). The static transfer and output characteristics are the same as the C-HEMT, and the total switching loss at 500 kHz is increased less than 7.8%. In addition, we investigated the impact of the PR layers' length, thickness, doping density on the performance.

Author Contributions: Methodology, H.W.; investigation, H.W., Y.S., Y.X., and C.L.; writing—review and editing, Y.S., and Y.X.; supervision, G.L.; project administration, Y.H. All authors have read and agreed to the published version of the manuscript.

Funding: This work was supported by the National Key R&D Program of China (No. 2020YFF0218503).

Institutional Review Board Statement: Not applicable.

Informed Consent Statement: Not applicable.

Data Availability Statement: Not applicable.

Conflicts of Interest: The authors declare no conflict of interest. The funders had no role in the design of the study; in the collection, analyses, or interpretation of data; in the writing of the manuscript, or in the decision to publish the results.

References

1. Chen, W.; Wong, K.-Y.; Chen, K.J. Single-Chip Boost Converter Using Monolithically Integrated AlGaIn/GaN Lateral Field-Effect Rectifier and Normally Off HEMT. *IEEE Electron Device Lett.* **2009**, *30*, 430–432. [CrossRef]
2. Meneghini, M.; Cibin, G.; Bertin, M.; Hurkx, G.A.M.; Ivo, P.; Šonský, J.; Croon, J.A.; Meneghesso, G.; Zanoni, E. OFF-state degradation of AlGaIn/GaN power HEMTs: Experimental demonstration of time-dependent drain-source breakdown. *IEEE Trans. Electron Devices* **2014**, *61*, 1987–1992. [CrossRef]
3. Meneghini, M.; Hilt, O.; Fleury, C.; Silvestri, R.; Capriotti, M.; Strasser, G.; Pogany, D.; Bahat-Treidel, E.; Brunner, F.; Knauer, A. Normally-off GaN-HEMTs with p-type gate: Off-state degradation, forward gate stress and ESD failure. *Microelectron. Reliab.* **2016**, *58*, 177–184. [CrossRef]
4. Wang, H.; Wei, J.; Xie, R.; Liu, C.; Tang, G.; Chen, K.J. Maximizing the performance of 650-V p-GaN gate HEMTs: Dynamic RON characterization and circuit design considerations. *IEEE Trans. Power Electron.* **2016**, *32*, 5539–5549. [CrossRef]
5. Ishida, H.; Kajitani, R.; Kinoshita, Y.; Umeda, H.; Ujita, S.; Ogawa, M.; Tanaka, K.; Morita, T.; Tamura, S.; Ishida, M.; et al. GaN-based Semiconductor Devices for Future Power Switching Systems. In Proceedings of the 2016 IEEE International Electron Devices Meeting (IEDM), San Francisco, CA, USA, 3–7 December 2016.
6. Chen, K.J.; Häberlen, O.; Lidow, A.; Tsai, C.L.; Ueda, T.; Uemoto, Y.; Wu, Y. GaN-on-Si power technology: Devices and applications. *IEEE Trans. Electron Devices* **2017**, *64*, 779–795. [CrossRef]
7. Kim, J.G.; Cho, C.; Kim, E.; Hwang, J.S.; Park, K.H.; Lee, J.H. High Breakdown Voltage and Low-Current Dispersion in AlGaIn/GaN HEMTs with High-Quality AlN Buffer Layer. *IEEE Trans. Electron Devices* **2021**, *68*, 1513–1517. [CrossRef]
8. Duan, B.; Yang, L.; Wang, Y.; Yang, Y. Experimental Results for AlGaIn/GaN HEMTs Improving Breakdown Voltage and Output Current by Electric Field Modulation. *IEEE Trans. Electron Devices* **2021**, *68*, 2240–2245. [CrossRef]
9. Xin, Y.; Chen, W.; Sun, R.; Shi, Y.; Liu, C.; Xia, Y.; Wang, F.; Li, M.L.J.; Zhou, Q.; Deng, X.; et al. Analytical Switching Loss Model for GaN-Based Control Switch and Synchronous Rectifier in Low-Voltage Buck Converters. *IEEE J. Emerg. Sel. Top. Power Electron.* **2019**, *7*, 1485–1495. [CrossRef]
10. Zhao, X.; Xu, Y.; Jia, Y.; Wu, Y.; Xu, R.; Li, J.; Hu, Z.; Wu, H.; Dai, W.; Cai, S. Temperature-Dependent Access Resistances in Large-Signal Modeling of Millimeter-Wave AlGaIn/GaN HEMTs. *IEEE Trans. Microw. Theory Tech.* **2017**, *65*, 2271–2278. [CrossRef]
11. Das, S.; Kundu, S. Simulation to Study the Effect of Oxide Thickness and High-K Dielectric on Drain-Induced Barrier Lowering in N-type MOSFET. *IEEE Trans. Nanotechnol.* **2013**, *12*, 945–947. [CrossRef]
12. Park, P.S.; Rajan, S. Simulation of Short-Channel Effects in N- and Ga-Polar AlGaIn/GaN HEMTs. *IEEE Trans. Electron Devices* **2011**, *58*, 704–708. [CrossRef]
13. Singiseti, U.; Wong, M.H.; Dasgupta, S.; Swenson, B.; Thibeault, B.J.; Speck, J.S.; Mishra, U.K. Enhancement-Mode N-Polar GaN MISFETs with Self-Aligned Source/Drain Regrowth. *IEEE Electron Device Lett.* **2011**, *32*, 137–139. [CrossRef]
14. Pinchbeck, J.; Lee, K.B.; Jiang, S.; Houston, P. Dual metal gate AlGaIn/GaN high electron mobility transistors with improved transconductance and reduced short channel effects. *J. Phys. D Appl. Phys.* **2021**, *54*, 105104. [CrossRef]
15. Lu, B.; Saadat, O.I.; Palacios, T. High-Performance Integrated Dual-Gate AlGaIn/GaN Enhancement-Mode Transistor. *IEEE Electron Device Lett.* **2010**, *31*, 990–992. [CrossRef]
16. Synopsys. TCAD Sentaurus™ Tutorial. Available online: <http://www.sentaurus.dsod.pl/index.html> (accessed on 19 January 2022).
17. Wang, F.; Chen, W.; Xu, X.; Sun, R.; Wang, Z.; Xia, Y.; Xin, Y.; Liu, C.; Zhou, Q.; Zhang, B. Simulation Study of an Ultralow Switching Loss p-GaN Gate HEMT With Dynamic Charge Storage Mechanism. *IEEE Trans. Electron Devices* **2021**, *68*, 175–183. [CrossRef]
18. Lidow, A.; de Rooij, M.; Strydom, J.; Reusch, D.; Glaser, J. *GaN Transistors for Efficient Power Conversion*; John Wiley & Sons: Hoboken, NJ, USA, 2019.
19. Joshi, V.; Tiwari, S.P.; Shrivastava, M. Part I: Physical Insight Into Carbon-Doping-Induced Delayed Avalanche Action in GaN Buffer in AlGaIn/GaN HEMTs. *IEEE Trans. Electron Devices* **2019**, *66*, 561–569. [CrossRef]
20. Verzellesi, G.; Morassi, L.; Meneghesso, G.; Meneghini, M.; Zanoni, E.; Pozzovivo, G.; Lavanga, S.; Detzel, T.; Häberlen, O.; Curatola, G. Influence of Buffer Carbon Doping on Pulse and AC Behavior of Insulated-Gate Field-Plated Power AlGaIn/GaN HEMTs. *IEEE Electron Device Lett.* **2014**, *35*, 443–445. [CrossRef]
21. Chini, A.; Meneghesso, G.; Meneghini, M.; Fantini, F.; Verzellesi, G.; Patti, A.; Iucolano, F. Experimental and Numerical Analysis of Hole Emission Process From Carbon-Related Traps in GaN Buffer Layers. *IEEE Trans. Electron Devices* **2016**, *63*, 3473–3478. [CrossRef]

22. EPC. eGaN FET Datasheet. Available online: https://epc-co.com/epc/Portals/0/epc/documents/datasheets/epc2001_datasheet.pdf (accessed on 19 January 2022).
23. Cheng, Y.; Wang, Y.; Feng, S.; Zheng, Z.; Chen, K.J. Observation and characterization of impact ionization-induced OFF-state breakdown in Schottky-type p-GaN gate HEMTs. *Appl. Phys. Lett.* **2021**, *118*, 163502. [[CrossRef](#)]
24. Wang, F.; Chen, W.; Li, X.; Sun, R.; Zhang, B. Charge storage impact on input capacitance in p-GaN gate AlGaN/GaN power high-electron-mobility transistors. *J. Phys. D Appl. Phys.* **2020**, *53*, 305106. [[CrossRef](#)]